# *Chapter 3: Enhancement and segmentation of histopathological images of cancer using dynamic stochastic resonance*

## Abstract:

Pathologists face difficulty in cell image detection as uneven dye causes overlapping, blurring, low contrast as well as weak boundary detection. The proposed Discrete Cosine Transform (DCT) based Dynamic Stochastic Resonance (DSR) technique enhances the histopathological images of cancer. DSR utilizes the internal noise of image to enhance it and automatic threshold method detects the cells. DSR processes intensity component of decomposed Hue, Saturation and Intensity (HSI). The DSR processed image helps in the better segmentation of histopathological images of four types of cancer cells i.e. breast, cervix, ovarian and prostate cancer. The comparison of segmentation results were performed on the University of California, Santabarbara (UCSB) available breast cancer datasets for analysis. The algorithm has been applied to total twenty-two (22) breast cancer images including benign and malignant and compared with ROI segmented Ground Truth images to validate our proposed DSR based Otsu's thresholding method's performance. DSR based segmentation obtained better results with 0.776 average Correlation, 0.979 average Normalized Probabilistic Rand (NPR) index, 0.011 average Global Consistency Error (GCE) and 0.185 average Variation of Information (VI). This approach has the advantage to identify the target objects of noisy and low contrast images. Based on the comparative study, the proposed methodology performs better than the other conventional methods, as it obtained high Correlation, NPR, and low VI, GCE.

## 3.1 Introduction:

Histopathological images provide an informative view of the underlying tissue since the structure of the tissue is preserved in the preparation process. It deals with the minute structure of the tissue and provides information about abnormalities present in the cellular structure of the tissue and cells. For better detection of cancer, pathologists use histopathology images for examination of tissue structure of the patient. Currently, scrutiny of histopathological images is the routinely used method to examine biopsy sample for the diagnosis of cancer (Fischer *et al.,* 2008; Lillie *et al.,* 1954). Moreover, diagnosis from histopathology images is considered to be the 'gold standard' in diagnosing a large number of diseases including, but not limited to many types of cancer (Rubin *et al.,* 2008).

Images obtained from different imaging modalities are contaminated with noise, low contrast and artifacts. Image pre-processing of histopathological images is an important step in medical diagnostic imaging as it influences the detection and classification of diseases. Primarily, the noises in histopathological images originate from procedural staining artifacts and nuclei debris (Arif *et al.,* 2007). Histopathological images generally contain many types of noises and artifacts in the captured image such as additive noise, gaussian noise, multiplicative noise, speckle noise, salt and pepper noise, random and periodic noise (Cohen *et al.,* 2015; Sadimin, *et al.,* 2012), which leads to poor quality of image.

Prior to further processing, the labelled images undergo contrast-enhancement and quality adjustment related steps. The main purpose of the pre-processing steps includes reduction of the background noises cum non-uniformities, improvement of finer details, and enhancement of image quality for accurate determination of Region of Interest (ROI) (Rolls *et al.,* 2010; Gonzalez *et al.,* 2004). Subsequent to image pre-processing, the output of the enhanced images serves as the input for other automated image processing techniques such as **(a)** segmentation, **(b)** features extraction and **(c)** classifications for Computer Aided Diagnosis (CAD) technique based systems (Dougherty 2009; Gonzalez *et al.,* 2002; Dhawan *et al.,* 2003). The above-mentioned processes aids in avoiding misclassifications due to variation in result caused by the presence of noise, artifact, staining, poor visibility, weak boundary detection, uneven dying, overlapping of cells, low contrast and blurriness respectively (Dermir *et al.,* 2005).

## 3.2 Enhancement:

Image enhancement is required for better visualization of dark images to improve visual perception, and to enable accurate interpretation. Many images have very low dynamic range of the intensity values because of insufficient illumination, and therefore need to be processed before being displayed. The image enhancement will produce enhanced edges and better quality images free from noise impacts that contribute towards minimizing the blurring effects.

The enhanced images will aid in edge detection and image quality refinement. Edge detection will direct towards originating the precise position of abnormalities present in cells (Plissiti *et al.*, 2011; Madabhushi, 2009; Malik *et al.*, 1990). Further, the design and analysis of efficient algorithms for each step of CAD system executes the significant function in deciding the efficacy and correctness of the overall CAD system. Image enhancement plays an important role in the design and development of the CAD system. The better image enhancement techniques are applied prior to segmentation process, for highlighting and enhancing the details of the abnormalities in the histopathological image such as size, irregular shape etc. that further reduce the False Positive (FP) during cancer detection. Hence, image enhancement is very essential and important step that determines the sensitivity of the overall CAD system. The enhanced image used for segmentation aims at splitting an entire image into a set of region is supposed to have the following properties: circularity regularity and boundaries, homogeneity in terms of colour and texture, and differentiation from neighbour regions (Rahmadwati *et al.*, 2012; Gurcan *et al.*, 2009).

The enhancement approaches present a large number of options for enhancing the visual feature of images (Maini *et al.*, 2010; Gonzalez *et al.*, 2002). The standard purpose of image enhancement is to develop an image for extraction of essential information. Further, this information acts an improved input for other automated image processing techniques (Gupta *et al.*, 2014; Jagatheeswari *et al.*, 2009).


**Figure 3.1: Basic enhancement process (Gupta *et al.*, 2009).**

Image enhancement simply means, transforming an image *"f"* into image *"g"* using *"T"* (where "*T"* is the transformation of the image). The values of pixels in images *"f"* and "*g"* are denoted by "*r"* and "*s"* respectively. As said, the pixel values "*r"* and "*s"* are related by the expression,

$$s = T(r) \qquad (3.1)$$

where "*T*" is a transformation that maps a pixel value "*r*" into a pixel value "*s*". The results of this transformation are mapped into the gray scale ranges as we are exploring with grayscale digital images only. Accordingly, the results are mapped back into the range (0, L-1], where L=2k, k being the number of bits in the image under considerations (Maini *et al.* 2010). Henceforth, for instance, in an 8-bit image, the range of pixel values will extend within (0, 255).

The pre-processing steps such as **(a)** de-noising and **(b)** contrast enhancement play a significant role in histopathological image analysis to recognize and analyze the cells structure and shape, etc. Henceforth, the pre-processing method improves the interpretability or perception of information by eliminating the noise present in the images for significant analysis (McAndrew *et al.,* 2014; Zhang *et al.,* 2004). The brief descriptions about denoising and contrast enhancement are as follows:

### 3.2.1 Denoising:

Images produced by histopathological needs denoising and enhancement for better diagnosis or further processing such as segmentation (Domingo *et al.,* 2008; Prayitno *et al.,* 2006). Denoising steps are used to reduce and remove noise from the image and to enhance features of interest for easier and more accurate analysis (Dermir *et al.,* 2005; Gonzalez *et al.,* 2002).

Common noise in histology images is blood cells and artifact stains in the background (Rolls *et al.,* 2010). The image that is gathered in digital format exhibits noise. The quality of the images will affect the accuracy of the diagnosis (Dermir *et al.,* 2005). To improve the visual quality of images, image enhancement techniques provide a variety of ways like deblurring, smoothing, improving contrast, denoising, (removing unwanted noise), sharpening, and unsharp masking etc. (Takashi *et al.,* 2009; Jain, 1989).

The removal of noise from the given image is an usual process. Various types of noises are present with large number of optical characteristics represented as multiple tags, artifacts arisen during sample screenings, background shadow lines depicting as parallel in a row strips etc. Such extraneous noises are eliminated for better achievement of results from CAD based systems.

The hunt for an efficient de-noising technique is an open challenge in the area of image processing. Massive development has been observed in this area; however effective algorithms with required applications are still not available. Commonly, shortcomings exist in eliminating fine structures and artifacts from the images (Bhattacharjee *et al.,* 2014; Cohen *et al.,* 1995; Zhang *et al.,* 2000; Gurcan *et al.,* 2009). Denoising technique includes the filtering process for reducing the noise and to enhance the image with an improvement. The accuracy of diagnosis depends on the quality of images and the elimination of noise. A number of de-noising methods proposed for enhancing the image such as median filter, mean filter, low-pass filter (LPF), high-pass filter (HPF), thresholding, adaptive filtering, gaussian filtering, homomorphic filtering and morphological operation etc. to eliminate and filter noises by various researchers (Rahmadwati *et al.,* 2010; Gonzalez *et al.,* 2004; Li *et al.,* 2007; Dermir *et al.,* 2005; Luck *et al.,* 2003). Many medical images consist of a background and region of interest (ROI) and denoising can separate these (Moulin *et al.,* 1999).

Image filtering is a pre-processing method to suppress frequencies of images with preservation of image properties. In image processing, filtration is an important part of the image quality enhancement. It removes artifacts and cancels noises that may interfere with histology images (McAndrew *et al.,* 2014). Such method in spatial domain for image filtering, the neighborhood pixels for any given pixel input contribute to assign a new output pixel in an image. Henceforth, the filtering is commonly applied to reduce image noises including variable noises (other objects not contained within the (ROI)) from the background. Histogram equalization is used to ensure illumination invariance. The background correction method can be applied to solve the luminance problem. The most commonly used method described in the literature is the threshold-based approach. This method compares pixel intensities where noise is defined by a value of the declared threshold (Dermir *et al.,* 2005).

Some researchers had applied the median filter method in the preprocessing process for medical images (Rahmadwati *et al.,* 2012; Li *et al.,* 2008). The median filter sorts the value (according to the brightness or intensity) of each neighboring pixel in ascending order (Yang *et al.,* 1995; Rahmadwati *et al.,* 2012). Subsequently, the median value of this ordered sequence is selected. The output pixel is formed by the median of neighborhood pixel.

However, the noise or dirt in the original image, such as salt and pepper noise, is removed and the sharpness of the image reduced. Median filters are suitable for pre-processing of histopathological images as their performance is particularly good for removing random and periodic noises (Gonzalez *et al.,* 2002; Luck *et al*., 2003). By using different high or low pass filters sharpening of the image achieved. Noise is filtered out utilizing various filters to sharpen the image edges. This de-noising step aids in the clear detection of cell boundary lines (Li *et al.,* 2008).

The design of unsharp masking is to subtract a scaled unsharp version of the image from the original. The result of unsharp masking appears to be a better image than the original; the edges are crisper and more clearly defined. The images, however, appeared to be much clearer to the human eye and perhaps to any pathologist. This can be explained by the fact that unsharp masking only deals with the edges in an image and therefore does not alter significantly the surfaces with important textural information. The usefulness of this image enhancement technique might be more appreciated when the morphological analysis is undertaken later in the study. Henceforth, unsharp masking is called 'edge enhancement' that results in enhanced edge pixel values (Dermir *et al.,* 2005; McAndrew *et al.,* 2004). Ling *et al.* (2002) denoised the low signal-to-noise ratio (SNR) molecular images using median diffusing algorithms. Alexandrov *et al.* (2010) presented edge preserving denoising to reduce pixel to pixel variability for better segmentation of matrix-assisted laser desorption imaging.

### 3.2.2. Contrast Enhancement:

Contrast enhancement is one of the most important technique for image enhancement (Kotkar *et al.,* 2013). In this technique, the contrast of an image is improved to make the image better for human vision. The term contrast, as observed in digital images, is the separation of dark and bright areas present in the image. Contrast enhancement method includes **(a)** Gamma (ϒ) correction, **(b)** Single Scale Retinex (SSC), **(c)** Contrast Limited Adaptive Histogram Equalization (CLAHE) (Gonzalez *et al.,* 1977).

The Gamma (ϒ) correction algorithm is utilized for coding and decoding the luminance (gray) or tri-stimulus (color) values as present in motionless images. The gamma values are adjusted to contrast with other still images for facilitating the identification of ROI zone in histopathological image slide (Veeramanikandan *et al.,* 2013; Belsare *et al.,* 2012).

Single Scale Retinex (SSC) provides either dynamic range compression (small scale), or tonal rendition (large scale) at a time. Application of this method leads to contrast enhancement of an image (Jobson *et al.,* 1997).

CLAHE algorithm improves the image contrast by improving the local contrast present in an image and by enhancing the weak boundary edges in each pixel of an image through limited amplification (Pisano *et al*., 1998; Zuiderveld *et al.,* 1994; Srivastava *et al.,* 2013).

## 3.3 Segmentation:

The segmentation process extracts the ROI and locates the suspicious region that contains the irregular shape and varying size of cells to determine the level of malignancy in a histopathological image (Belsare *et al.,* 2012; Madabhushi *et al.,* 2009). Image segmentation is a crucial part in making accurate useful information and characteristics of the ROI from images for computer-aided diagnosis of cancerous cells. Each segmentation method varies in its performance depending on the types of application and image modality (Dermir *et al.,* 2005).

However, the accuracy of segmentation largely depends on preprocessing steps (Rahmadwati *et al*., 2010). Segmentation is the process of dividing an image into a region having similar properties such as gray level, color, texture, brightness, and contrast (Gonzalez *et al.,* 2004; Pratt, 2001; Pal *et al.,* 1993). In pathology, segmentation of histopathological sections is the ubiquitous requirement due to the large variability of histopathological tissues. Further, machine learning techniques play a vital role in delivering superior performance over standard image processing methods. During image analysis, the segmentation process is an essential domain. It is used to locate objects and boundaries in an image (Sharma *et al*., 2009).

The basic purpose of segmentation is to extract the important features from the image and perceive the information. Selection of appropriate segmentation method depends on the type of features, which has to be preserved for detection. Segmentation of cells from the background for qualitative comparison mainly utilizes **(a)** Otsu's thresholding **(b)** k-mean clustering **(c)** Fuzzy c-mean clustering.

### 3.3.1 Otsu's Thresholding:

Threshold method is widely used in medical image segmentation (Keenan *et al*., 2000; Arif *et al*., 2007; Stoitsis *et al*., 2006; Dougherty, 2009). One of the well known threshold method is the Otsu method, which is based on statistical analysis of variance. This method is conducted by maximizing the separation of image histogram partitions into two classes before deciding on the threshold. It means that the variances in the two classes should be as small as possible (Otsu *et al*., 1979). Otsu's method used for bi-level thresholding on intensity values of Hue, Saturation, and Intensity (HSI) decomposed image (Stoitsis *et al*., 2006; Zhou *et al*., 2000). The Ostu's thresholding image segmentation (Otsu *et al*., 1979; Sezgin *et al*., 2004) method is based on gray level thresholding, which computes a global threshold level, that is used to convert a gray level image to binary image. The threshold level lies in the range (0, 1]. Gray-level thresholding uses Otsu's method that chooses the threshold to minimize the interclass variance of the thresholded black and white pixels. Liu *et al.* (2007) introduced the microscopic image analysis with the help of adaptive threshold segmentation. Phukpattaranont *et al.* (2008) presented an algorithm for image segmentation by using a neural network. Naik *et al.* (2008) divided pixel values into low level and high level information between object pixels and the background pixels discrimination to segment cancer cells.

Thresholding approaches use a value (threshold) to separate the objects from the background. This value is typically based on image intensity or its transforms such as Fourier descriptors or wavelets (Sahoo *et al.,* 1998; Sezgin *et al.,* 2003). The threshold is usually recognized to satisfy some constraints or to optimize certain objective functions.

For example, generally used Otsu's method finds the threshold to maximize the between-class variance (Gonzalez *et al.,* 2008). For microscopic biopsy image segmentation, multi-thresholding approaches are mostly used to extract objects of different classes, e.g., nuclei, cytoplasm, stroma, and background (Loukas *et al.,* 2004; Gonzalez *et al.,* 2004).

The multilevel thresholding is necessary to extract different objects from histology images. For example, in the case of *K* object classes ($s_1, s_2, \ldots, s_K$) in a digital image I of size *(X × Y)*, Otsu's method finds the thresholds that maximize the between class variance given in Equation (3.2)

$$\sigma_B^2 = \sum_{k=1}^{K} P_k(\mu_k - \mu_G) \qquad (3.2)$$

where

$$P_k = \sum_{1 \,\epsilon\, s_k} P_1 \qquad (3.3)$$

$P_1$ is the normalized histogram (probability) of intensity l, i.e., $P_1 = n_1/\mathrm{XY}$, and $n_1$ is the number of pixels with intensity l . $\mu_k$ is the current mean of $s_k$,

$$\mu_k = \left(\frac{1}{P_k}\right) 1P_1 \qquad (3.4)$$

and $\mu_G$ is the whole image intensity mean. The K classes are separated by K − 1 thresholds that maximize $\sigma_B^2$.

### 3.3.2 k-means clustering:

Clustering is a method that classifies an object into a group, or cluster, according to the measure of object similarity, intensity or texture (Dermir *et al.,* 2005). The clustering process involves quantitative, objective assessments in order to group objects into a cluster by similarity measurement. The common measurement used for measuring similarity is the distance measure such as Mahalanobis distance, Euclidian distance and Manhattan distance (Dermir *et al.,* 2005). k-means clustering is a popular clustering method used in image segmentation and in this chapter, the following sub-sections elaborates its applications. k-means clustering is one of the simplest methods of clustering. The algorithm of k-means clustering is used to classify an image based on its features (texture or color features). The process of clustering is achieved by measuring the sum of the distance between the data and the cluster centroid (Ilea *et al.,* 2006). In this method, the number of clusters is predefined. The general algorithm of k-means clustering is as follows:

1. Assuming *k* classes, randomly select the *k* starting cluster centers from the set of feature vectors $\{(x_1, x_2, \ldots, x_N)\}$ in the m - dimensional feature space.
2. Assign all other feature vectors to the cluster center $\mu_j$ to which they are closest, using a distance measure such as the Euclidean distance:

$$D_j(x) = \sqrt{\sum_{i=1}^{m} \left(x_i - \mu_j\right)^2} \qquad (3.5)$$

3. Update the position of each cluster center $\mu_j$ as the center of gravity of the corresponding cluster, calculated as the mean of the $N_j$ feature vectors currently assigned to that cluster, that is

$$\mu_j = \frac{1}{N_j} \sum_{x \,\epsilon\, w_j} X_j \qquad j = 1,2, \ldots\ldots\ldots W \qquad (3.6)$$

4. The second and third steps are repeated until convergence, that is, until no assignments change.

### 3.3.3 Fuzzy c-means clustering:

In this algorithm, the test pixel is allowed to be the member of two or more clusters with different membership coefficient. Fuzzy c-means (FCM) algorithm is iterative in nature, generates fuzzy partition matrix, and requires cluster center along with objective function. The values for cluster center and objective function are updated at every single iteration and are stopped when the difference between two successive objective function value is less than some predefined threshold value. The objective function and the algorithm are given as follows (Yang, 2005).

The FCM clustering algorithm was first introduced by (Dunn, 1973) and then extended by (Bezdek, 1975).

The FCM algorithm is as follows:

Let X = $\{x_i\}$ an image, i = {1, 2, 3,.....n} where $x_i$ are the pixels of X and n is the total number of pixels.

The FCM algorithm minimizes the objective function (Bezdek, 1975):

$$J_{FCM} = \sum_{i=1}^{c}\sum_{k=1}^{n} \mu_{ik}^{m} d^2(x_k, V_i) \qquad (3.7)$$

where $\mu_{ik}$ is the membership function matrix, d the Euclidian distance metric between $x_k$ and the cluster center $V_i$ and $m$ is the degree of fuzziness (m > 1). The membership function $\mu_{ik}$ is the heart of the FCM, where the membership degrees are given by:

$$\mu_{ik} = \frac{1}{\sum_{j=1}^{c}\left(d_{ik}/d_{jk}\right)^{2/(m-1)}} \qquad (3.8)$$

The cluster centers are:

$$V_i = \frac{\sum_{i=1}^{n} \mu_{ik}^{m} x_k}{\sum_{k=1}^{n} \mu_{ik}^{m}} \qquad (3.9)$$

The choice of a distance which metric in clustering problems is crucial. The Euclidean distance metric is widely used because of its simplicity, the hypothesis that the data are uncorrelated and the clusters have super spherical shapes, which are not possible in image segmentation; therefore, the Mahalanobis distance is more suitable. Sharma *et al.* (2009) used annealing based FCM algorithm, modeled as graph search method for segmentation of the medical image (Zhang *et al.*, 2004; Bezdek, 1975).

### 3.3.4 Dynamic Stochastic Resonance:

Typically, the enhancement of low contrast noisy images is challenging as noises degrade signal performances. For that reason, researchers used to screen it out (Bhattacharjee *et al.*, 2014). Several techniques are proposed for de-noising, enhancement, and segmentation of histopathological images, in order to increase the contrast between the cells and tissues. However, these methods not capable of improving the desired image contrast and distortion of the image information contents. Further, simple linear de-noising methods used to degrade the image details and edges (Belsare *et al.*, 2012; Dermir *et al.*, 2005; Gurcan *et al.*, 2005). In the context of the above-mentioned techniques, we have proposed DSR based method for image contrast enhancement by denoising the images in a single step.

**The fundamental theory of Dynamic Stochastic Resonance:**

DSR is a noise induced phenomenon. It occurs when noise enhances the performance of signal in a nonlinear system. It is effective for enhancement and denoising of low contrast images. The noise present in the image decreases when it interacts with a nonlinear dynamic system. In other words, noise is useful when combined with a nonlinear dynamical system. DSR is the signal information in a non linear system in the presence of an appropriate amount of noise, which is greater than the signal information alone in the nonlinear system (Gammaitoni *et al.*, 1998; Jung, 1991; McNamara *et al.*, 1989; Fauve *et al.*, 1983). Stochastic Resonance (SR) helps to amplify a weak signal with the help of appropriate level of noise in the presence nonlinear system. The following three conditions lead to occur in SR phenomenon **(a)** signal of low amplitude, **(b)** appropriate level of noise and **(c)** non-linear system with a threshold (Gammaitoni *et al.*, 1998).

In this method, a sufficient amount of noise and signal of low amplitude together cross the threshold of a non linear system. The noise, which is added to the weak signal, must be high enough that a system can change its state by crossing the threshold value. However, the large amount of noise may lead to oscillations between two states and degrades the performance whereas the low amount of noise is incapable of changing the state (Gammaitoni *et al.*, 1998; McNamara *et al.*, 1989). The first experimental work on visualization of SR was reported in (Ryu *et al.* (2011).

Quartic bi-stable model of SR has been used Fourier transform coefficient of the image and found valuable for diagnosing of brain lesions in MRI (Rallabandi *et al.*, 2010). The wavelet transform based SR enhanced the appearance of sonar images; followed by fuzzy c-means was used to extracting the ROI to calculate the position of obstacle (Banerjee *et al.*, 2014). The drawbacks of these methods were non-optimum DSR parameter values and sophisticated selection of the number of iterations. However, few studies used the approaches of optimum DSR parameter for MRI data using Quartic bi-stable model and potential neuron model of SR (Singh *et al.*, 2017; Singh *et al.*, 2016).

Our investigation includes the utilization of internal noise of an image for the purpose of contrast enhancement in spatial domain. DSR process includes intensity component of decomposed Hue, Saturation, and Intensity (HSI). Henceforth, the DSR technique utilizes the noise associated with the image itself to enhance the image quality. The present study explores the effects of different image transformation methods that work as the input source to DSR based image enhancement techniques. Various histopathological images of different cancerous tissue undergoes image processing, resulting in the poor state pixels transition to enhanced pixel states. The characteristics of DSR based processes aids in image contrast enhancement using the internal noise of the images.

**Dynamics of Quartic Bi-stable based SR System:**

The signal information in the non-linear system in the presence of appropriate noise is greater than the signal information alone in the non-linear system (Gammaitoni *et al.*, 1998; Jung, 1991). Many non-linear dynamics involved in SR phenomena were presented in the last three decades. (McNamara *et al.*, 1989; Fauve *et al.*, 1983). Quartic bi-stable is one of the most famous models of SR system. The dynamic equation obtained with the help of Langev in equation (Coffey *et al.*, 2012):

$$\frac{d}{dt}x(t) = -\ \frac{d}{dt}U\ (x,t)s(t)\ n(t) \qquad (3.10)$$

where $U\ (x,t)$ is quartic potential, $s\ (t)$ is input signal and $n\ (t)$ is the added Gaussian white noise (with zero mean) to the system.

$$U(x,t) = -a\frac{x^2}{2} + \ \mathrm{b}\frac{x^4}{4} \qquad (3.11)$$

where a > 0, b > 0 are bi-stable double well parameters. The Brownian particle in this double well system will have two stable states at points: $x_m = \pm\sqrt{\frac{a}{b}}$ and one metastable at $x = 0$. As shown in Figure 3.2, the particle has to cross potential the barrier $\Delta U = \frac{a^2}{4\,b}$ to acquire one stable state to another. The final dynamic equation for SR after replacing the value of $U(x,t)$ in (3.10) is:

$$\frac{d}{dt}x(t) = ax - bx^3\ + s(t) + n(t) \qquad (3.12)$$

Here, $s(t) + n(t)$ term can be written as $input$, because the study considered $n(t)$ as the internal noise of input image itself. Equation (3.12) can be rewritten and discretized in $k$ steps using Euler-Maruyama's method:

$$x(n+1) = x(n) + k\ (a\ x(n) - b\ x^3(n) + input\ ) \qquad (3.13)$$

There are two assumptions for SR phenomena: the strength of the input signal must be less than the potential barrier to maintain bi-stability of the system. In the absence of noise, there is no switching occurs. After adding the noise, switching must occur as noise added system crosses the barrier height. Figure 3.2 (a) shows double well-unforced quartic potential for $a = 4$, $b = 1$, which helps to get minima at $x_m = \pm 2$ and $\Delta U = 4$ and figure 3.2 (b) shows modulated system in the presence of sufficient amount of energy i. e. noise intensity.

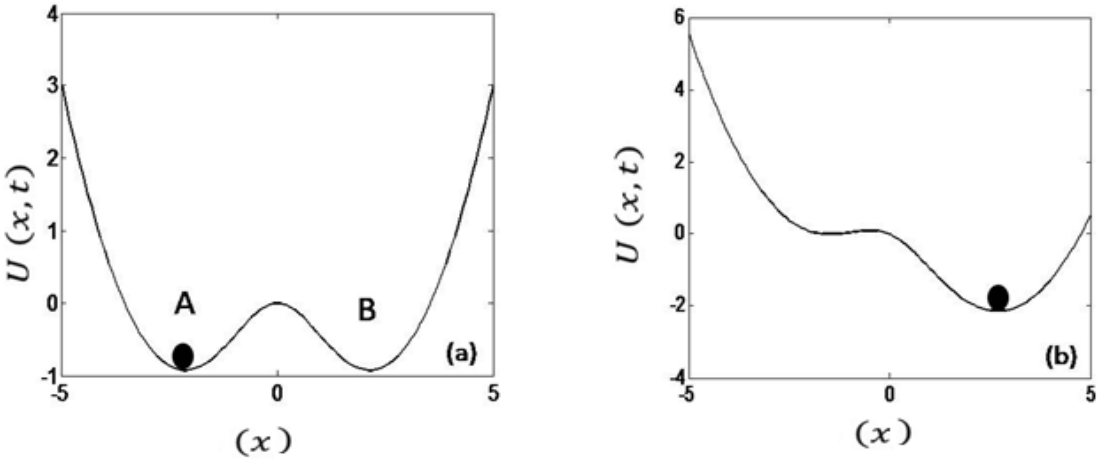


**Figure 3.2: Quartic bi-stable based DSR system.**
(a) Quartic potential for the unmodulated system at $t = 0, n(t) = 0$, (b) modulated system in presence of sufficient amount of energy i. e. noise intensity

Quartic bi-stable model was used for DSR in most of the previous studies for either image enhancement or segmentation but the other DSR models can also be applied to different image processing applications that depend on characteristics of input images, associated noise with it and the desired outcomes (Gammaitoni *et al.*, 1998; Fauve *et al.*, 1983).

**Discrete Cosine Transform:**

The spectral separation property of Discreet Cosine Transform (DCT) domain helps to enhance the image features as it treats various frequency components independently. Transformed image $I(k_i,k_j)$ obtained after applying 2-D DCT on input image $I(i,j)$ defined as:

$$I(k_i, k_j) = \left(\frac{2}{N}\right)^{\frac{1}{2}} \left(\frac{2}{M}\right)^{\frac{1}{2}} \sum_{i=0}^{N-1} \sum_{j=0}^{M-1} \Lambda(i)\Lambda(j)\, I(i,j)$$

$$\times \cos\frac{(2i+1)k_i\pi}{2M} \cos\frac{(2j+1)k_j\pi}{2N} \qquad (3.14)$$

$$\Lambda(i) = \begin{cases} \frac{1}{\sqrt{2}} & for\ \xi = 0 \\ 1 & otherwise \end{cases}, \ \Lambda(j) = \begin{cases} \frac{1}{\sqrt{2}} & for\ \xi = 0 \\ 1 & otherwise \end{cases}$$

where the size of the input image is N×M. The transformed image $I(k_i,k_j)$ serves as input to DSR. So the final dynamic equation for SR system for image enhancement is:

$$x(n+1) = x(n) + k\,(a\,x(n) - b\,x^3(n)) + \ \mathrm{I'(k_i k_j)} \qquad (3.15)$$

## 3.4 Materials and Methods:

For the enhancement and segmentation of the cells, we have acquired the images of cancerous tissues from the following histopathological procedure. The present study includes tissue preparation of histopathological stained images of various types of cancer cells i.e. cervix, ovarian, breast, and prostate cancer. The experiments were performed at S. S. Hospital and Research Centre, Patna with the consent of patients. The ethical committee of the above mentioned institute had approved the investigation procedures and are provided in appendix-5(a) and 5(b) respectively.

### 3.4.1 Preparation of histopathological slide:

The histopathological slide preparation techniques normally consist of following steps **(1)** tissue fixation, **(2)** tissue processing **(3)** embedding and block preparation **(4)** sectioning and slide preparation **(5)** staining for the acquisition of images. The steps in the preparation of tissue slide are depicted in figure 3.3

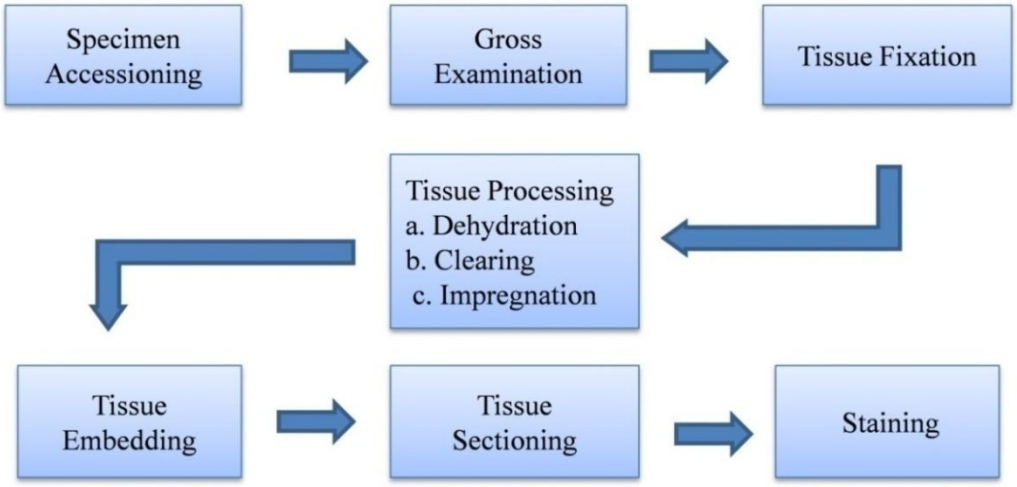


**Figure 3.3: Basic steps for slide preparation for histopathological image.**

**Tissue fixation:**

Fixation is the primary step of tissue processing. Fixation was done to prevent decay and to stabilize the tissue cell components. Immediately tissues were washed and transferred into 10% neutral buffered formalin for their fixation for 24 hours. The formalin fixed tissues were washed overnight under running tap water for 24 hours to allow paraffin wax to infiltrate into the tissue easily.

**Tissue processing:**

Figure 3.4 shows the following steps in the tissue processing methods with the help of automatic tissue processor.

**Dehydration**: Washed tissues were further processed to dehydration with increasing concentration of alcohol gradient as 30%, 50%, 70%, 90%, and 100%. Each alcohol gradient was used for 30 minutes.

**Clearing/Hydration**: Dehydration was checked by immersing the tissues in xylene for 10-30 minutes. The presence of water shows milky white colour when exposed to xylene. If water was present in tissues they were again put in the absolute alcohol.

**Impregnation:** Washed tissues were infiltrated by two changes of paraffin wax that is first put in 1:1 solution of xylene + wax for 45 minutes and after that pure paraffin wax and left for 45 minutes to 2 hours at 45 ± 50ºC.


**Figure 3.4: Tissue processing step.**
(a) Tissue sample. (b) After grossing sample present in the box was kept in the container for tissue processing. (c) Automatic tissue processor.

**Tissue embedding and block preparation:**

'L' shape-mould used to make paraffin wax block which holds the tissue specimen. The processed tissues were embedded in molten paraffin wax poured into the L- moulds at 55-60˚C. The air bubbles were removed with the help of a hot pointed needle and blocks were made. After complete solidification, the blocks were removed and stored for 24 hours in a refrigerator in small labelled paper bags before use as shown in figure 3.5.

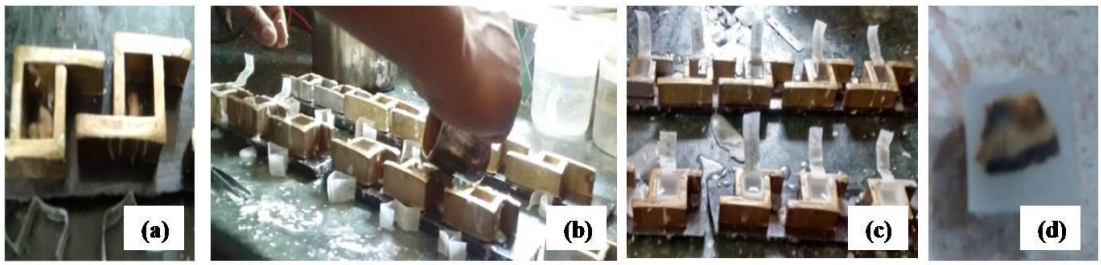


**Figure 3.5: Steps for block preparation.**
(a) Tissues in L-mould shape block. (b) Pouring of melted wax (55-60˚C) in the blocks contain tissue sample. (c) Solidification of block (d) Prepared block. Tissue sectioning and slide preparation:

The paraffin block having tissue was attached in the rotary microtome. The rotary microtome was used for sectioning of tissue blocks with the thickness of 3-5µm. The sections were carefully picked from the knife by a forceps which float in a water-bath of 50 to 55˚C (slightly below the melting point of wax) to remove folds in the sections.

Unfolded sections were picked by clean microscopic glass slides and were placed in an oven maintained at a temperature of 50$^{o}$C for 20-30 minute for proper drying and better adhesion. At this stage, the sections were ready for staining as shown in figure 3.6.


**Figure 3.6: Tissue sectioning and slide preparation step.**
(a) Tissue sectioning by microtome. (b) Section kept in the water bath for proper spreading. (c) Sections transferred to the slide.

**Hematoxylin and eosin staining:**

To visualize different components of the tissue under a microscope, the sections were dyed with one or more stains for highlighting them. The objective of staining is to enhance the contrast and highlight specific intra or extracellular structures under the microscope. Staining methods provide details of structure and organization, by the proper treatment of the section with various dye solutions. The nucleus is acidic in nature and has an affinity for basic dyes while the cytoplasm is basic and has the affinity for acidic dyes. Therefore, two different dyes, one Haematoxylin (basic) and eosin (acidic) are used to differentiate the cellular structures, such as nucleus and cytoplasm. Haematoxylin stains DNA rich nuclei in blue, while eosin stains cytoplasm in dark pink shade, muscle in a medium pink shade, stroma and connective tissue in a light pink shade. For this purpose the sections on a slide were de-waxed by incubating in xylol, for about 30 minutes, followed by the second wash of xylene. Afterthat, rehydrated with graded series of alcohols 100%, 90%, 70%, 50% and 30% for 10-20 minutes.

Rehydration was followed by staining with Haematoxylin for 1-2 minutes, destaining in 1% acid solution. Again the sections were dehydrated in series of 30%, 50%, and 70% alcohols and stained in eosin for 2-5 min., washed twice in 70 % alcohol. After staining, dehydration was carried out at 90% then 100% ethanol. In 100% alcohol, the slides were kept a little longer (10-15 minutes) then cleared in clove oil, washed with xylol to remove the traces of clove oil. After that adequate amount of mountant Dibutyl Phthalate in Xylene (DPX) was put and the sections were covered with a cover slip. The slides were stored at room temperature in horizontal position till DPX hardens. Figure 3.7 (a) show the haematoxylin and eosin stained slide 3.7 (b) shows the magnified form of stained slide.

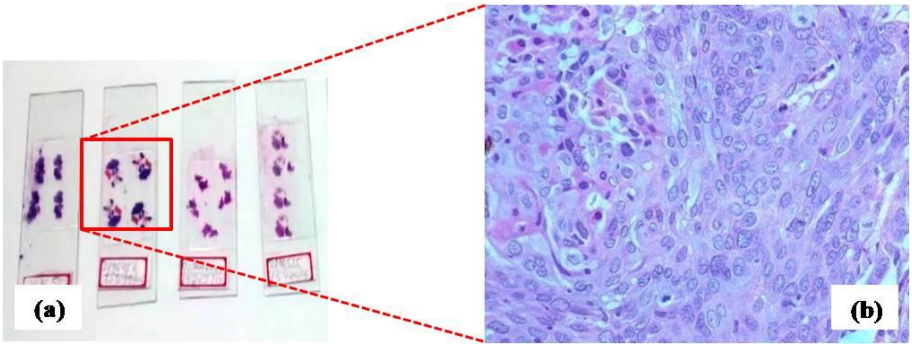


**Figure 3.7: Stained slide with haematoxylin and eosin.**
(a) Sample present on slide. (b) Photomicrograph of a cross section of the histopathological images of biopsy sample.

### 3.4.2 Image acquisition:

The images of tissue slides were captured using brightfield microscope Olympus CH 20I coupled to a CCD color camera, TOUPVIEW software and computer system Dell E19144/E20144 having processor Intel®Core TM i5-4590 CPU@3.30GH and 64-bit window 8.1 operating system. Microscope illumination system has a Philips halogen bulb of 6V 20 W types 7388. The size of the mechanical stage was 160(W) X 132(D) mm, and movement range was 76(H) X40 (V) mm. The obtained image was saved in .tiff format, having 2592 × 1944 pixel resolution. The sections of the tissue were examined at magnification of (40 x and 100 x) objectives using Olympus camera. The selected sections of different types of cancer cells were evaluated for histological changes. Figure 3.8 depicts the images which show low and high magnified benign and malignant breast cancer images.

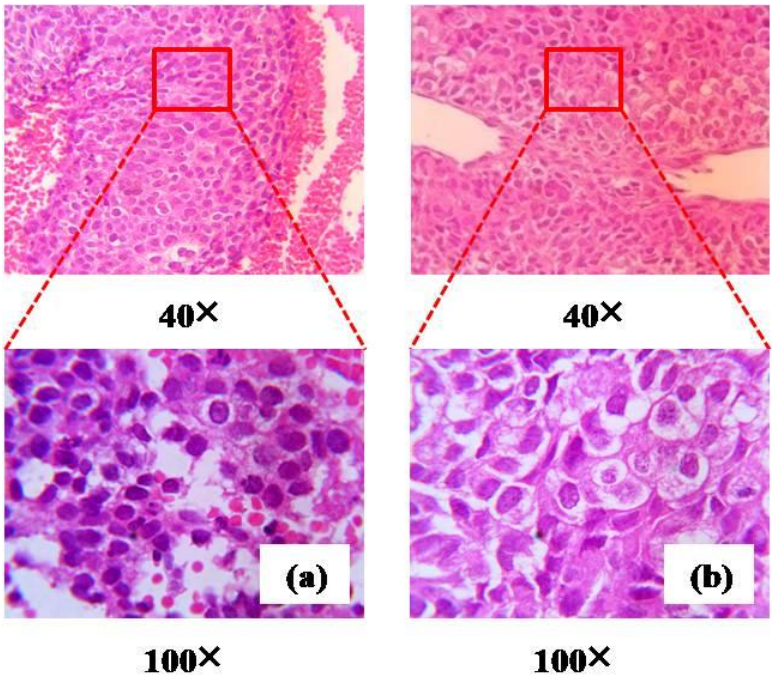


**Figure 3.8: Histopathological HE stained breast cancer images**
(a) Malignant cervix cancer, at 40x and 100x (b) Malignant breast cancer image at 40x and 100x.

The prepared histopathological images contain certain degrees of noises. Histopathology images are acquired from microscopes, henceforth, it may consist some deficient like uneven staining, low contrast, dust particles, air bubbles, and tissue folding. Pathologists face difficulty in cell image detection because of artefact, overlapping, and blurred, low contrast as well as weak boundary detection caused by uneven dyeing as shown in figure 3.9. Henceforth, for removal of acquired noises, we had undertaken various image enhancement techniques.

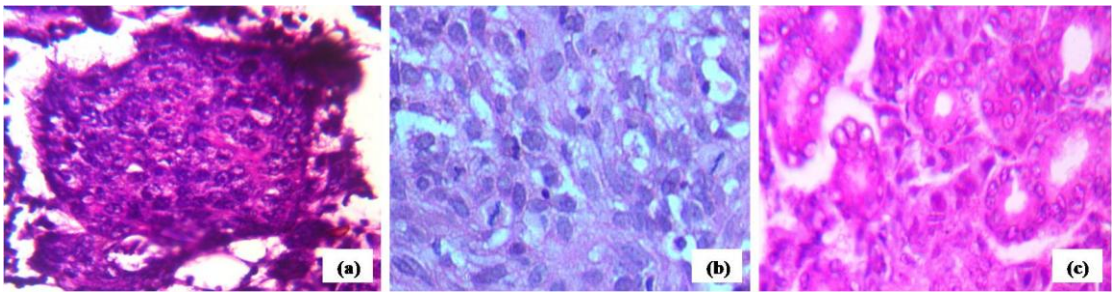


**Figure 3.9: Example of challenges in cells detection and classification.**
(a) Artifact (b) Overlapping (c) Heterogeneity

### 3.4.3 Algorithm for DSR based enhancement and segmentation:

In the present chapter, DSR based segmentation method is proposed for histopathological stained images of four types of cancer cells i.e. breast, cervix, prostate and ovarian cancer. Otsu's method used for thresholding on DSR processed intensity values of HSI decomposed image. Simple Otsu's, k-means, Fuzzy c-means image segmentation algorithms were compared with proposed methodology. It has been observed the DSR works well for the histopathological images having cells with a similar background. The comparison results reveal that the proposed DSR based Otsu's thresholding has a clear edge on considered segmentation techniques.

DSR utilizes the internal noise of image to enhance it and automatic threshold method detects the cells from the images. The obtained input images were transformed to DCT to demonstrate the effect of the input domains on enhanced image quality. The DCT used to change the domain of input image as it provides better energy compaction (Khayam *et al.*, 2003). Hence, we have used the coefficients of DCT for DSR processing. The discrete dynamics of DSR uses the step size, 0.01 to process the DCT coefficients of intensity component of the image. Finally, reconstruction of the images takes place to obtain the enhanced output image. This technique tunes the intensity values of the image according to the Quartic bi-stable double-well system parameters "$\boldsymbol{a}$" and "$\boldsymbol{b}$" and utilizes internal noise for the enhancement. The separate intensity component from the HSI space utilizes SR based enhancement on this component and afterward applies Otsu's thresholding on the SR processed output images. Eventually, the final step includes a combination of all the three frames respectively.

Figure 3.10 shows a generalized schematic block diagram of segmentation of low-contrast, noisy images based on DSR. This algorithm is used to identify a target object represented by a region of connected pixels. The proposed methodologies are implemented on PC with 3.4 GHz Intel Core i7 processor, 4GB RAM, and the entire image processing algorithms reported here were developed in the MATLAB®12 on Windows 8.1 platform.

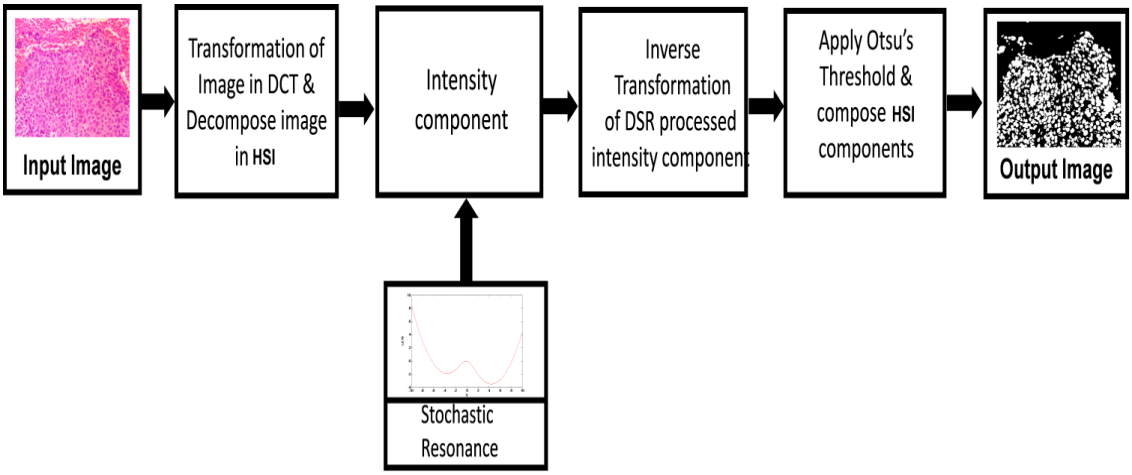


**Figure 3.10: Illustration of image segmentation using DSR.**

The algorithm steps are as follows:

**Step 1** Compute HSI decomposition of DCT transformed input image.

**Step 2** Application of DSR to intensity component (*I'*) of an image.

a) Initialize $x(0) = 0, a = 2\sigma^2,\ b \leq \frac{4\,a^3}{27},\ k$

*where* σ is the mean of the image

b) Use iterative equation given in equation (3.13) to compute intensity value

$$x(n+1) = x(n) + k\,(a\,x(n) - b\,x^3(n) + I')$$

Repeat steps 2 (b) to get maximum performance of segmentation.

**Step 3** Compute inverse DCT of intensity value of image

**Step 4** Apply Otsu's method for bi-level thresholding on intensity value and merge it to another component.

**Step 5** Analyze performance measure of segmented image.

### 3.4.4 Segmentation performance matrices:

Several segmentation methods have been adapted for cytoplasm, cell, and nuclei segmentation from histopathology images utilizing threshold based, region based, and clustering based algorithms respectively. However, the selections of segmentation methods depend on the type of the features to be preserved and extracted. For the segmentation of ROI, the ground truth image is manually cropped and created from histology dataset (Al-Kofahi *et al.,* 2010). The DSR based Otsu's thresholding segmentation algorithms are used because of the preservation of the desired information (Gammaitoni *et al.,* 1998). The performance of various segmentations is quantified in terms of (a) Correlation, (b) Global Consistency Error (GCE) Martin et al., 2001) (c) Variation of Information (VI) (Unnikrishnan *et al.,* 2007) and (d) Normalized Probabilistic Rand (NPR) index (Unnikrishnan *et al.,* 2005) of the segmented image with the ground truth image. The brief description of these performance measures is as follows.

**Correlation:**

Correlation is a qualitative measure for the edge preservation. This parameter can be used to preserves the edges of the original image (Salinas *et al.,* 2007). Correlation implies a mutual relationship or connection between two or more things. Correlation is any of a broad class of statistical relationships involving dependence, though in common usage it most often refers to the extent to which two variables have a linear relationship with each other (Rodgers *et al.,* 1988; Dowdy *et al*., 1983). If we have a series of 'n' measurements of 'X' and 'Y' written as $x_i$ and $y_i$ for i = 1, 2, ..., n, then the sample correlation coefficient can be used to estimate the population Pearson correlation 'r' between X and Y. The sample correlation coefficient is written:

$$r_{xy} = \frac{\sum_{i=1}^{n}(x_i - \bar{x})\,(y_i - \bar{y})}{(n-1)\,s_z\,s_y} = \frac{\sum_{i=1}^{n}(x_i - \bar{x})\,(y_i - \bar{y})}{\sqrt{\sum_{i=1}^{n}(x_i - \bar{x})^2 \sum_{i=1}^{n}(y_i - \bar{y})^2}} \quad (3.16)$$

where $\bar{x}$ and $\bar{y}$ are the samples means of *X* and *Y*, and $s_x$ and $s_y$ are the sample standard deviations of *X* and *Y* (Francis *et al.,* 1999).

**Global Consistency Error (GCE):**

In research paper (Martin *et.al.* 2001) authors propose two metrics that can be used to evaluate the consistency pair of segmentations. These measures are designed in such a way that they are tolerant to refinement, i.e. if subsets of regions in one segmentation consistently merge into some region in the other segmentation the consistency error should be low. To compute the consistency error for a pair of images, at first a measure of the error at each pixel $p_i$ is defined as follows:

$$E\ (S_1, S_2, p_i)\ \ \frac{|R(S_1, p_i) \backslash R(S_2, p_i)|}{|R(S_1, p_i)|} \tag{3.17}$$

where, $R\ (S_j, p_i)$ is the region in segmentation j that contains pixel $p_i$,\ denotes set difference, and $|\ .\ |$denotes set cardinality. This error measure evaluates to 0 if all the pixels in $S_1$are also contained in $S_2$ thus achieving the tolerance to refinement discussed above. This measure is not symmetric, so far every pixel it must be computed twice, once in each direction. Given the error measures E at each pixel, the two segmentation error measures namely local consistency error (LCE) and GCE defined by Martin *et al.*, 2001) reads

$$GCE\ (S_1, S_2) = \frac{1}{n}\ min\left\{ \sum_i E\ (S_1, S_2, p_i), \sum_i E\ (S_2, S_1, p_i) \right\} \tag{3.18}$$

And

$$LCE\ (S_1, S_2) = \frac{1}{n} \sum_i min\{\ E\ (S_1, S_2, p_i),\qquad E\ (S_2, S_1, p_i)\} \tag{3.19}$$

Since LCE < GCE, hence GCE is a tougher measure than LCE and that's why it is used in this thesis. A small value of GCE close to zero represents better segmentation. GCE quantify the amount of error in segmentation i.e. 0 signifies no error and 1 indicates no agreement.

**Variation of Information (VI):**

Variation of Information (VI) is a measure of the distance between two clusters (partitions of elements) (Unnikrishnan *et al.*, 2007). Clustering with clusters is denoted by a random variable, $X$, $X = \{1, \ldots, k\}$ such that $P_i = |X_i|/n$, $i \in X$, and $n = \Sigma_i X_i$ is the variation of information between two clusters $X$ and $Y$. Thus VI ($X$, $Y$) is represented using

$$VI\,(X,Y) = H\,(X) = H\,(Y) - 2I\,(X,Y) \qquad (3.20)$$

where $H\,(X)$ is entropy of $X$ and $I\,(X, Y)$ is common information between '$X$' and '$Y$'. VI ($X$, $Y$) measures the reduction in cluster assignment in clustering '$X$' into the uncertainty of item's cluster in clustering '$Y$'.

**Normalized Probabilistic Rand (NPR):**

Normalized probabilistic rand (NPR) is the nonparametric measure of goodness of segmentation algorithms (Unnikrishnan et al., 2005). Rand index between test 'S' and ground truth 'G' is estimated by adding the number of pixel pairs with the same label and some pixel pairs having different labels in both 'S' and 'G' then dividing it by a total number of pixel pairs. Given a set of ground truth segmentations $G_k$, the NPR is estimated using Equation (3.21) such that $c_{ij}$ is an event that describes a pixel pair $(i, j)$ having the same or different label in the test image test

$$\mathrm{NPR}\,(S_{\mathrm{test}}, \{G_k\}) = \frac{1}{(N/2)} \sum_{i,j\ \&\ i<j} [\, c_{ij}\, p_{ij} + (1 - c_{ij})(1 - p_{ij})] \qquad (3.21)$$

## 3.5 Results and discussion:

This study analyzes the effect of image transformations on DSR in terms of quality of histopathological images. Figure 3.11 depicts the qualitative comparison of various conventional image enhancement techniques such as gamma correction, CLAHE, SSR and proposed DSR based image enhancement for the histopathological image of cervix cancer. The ultimate goal of the work is to segment cells from the background using DSR and Otsu's thresholding. Henceforth, we have considered only intensity component of the original image to compare the enhancement performance. The figure 3.11 (f) depicts the DSR based image enhancement (our proposed methodology) with better suppression of the background Red Blood Cells (RBC) in comparison to other classical techniques as revealed from figure 3.11 (c) $\Upsilon$ correction with $\Upsilon$=1.1, 3.11 (d) SSR method, and 3.11 (e) enhancement using CLAHE respectively.

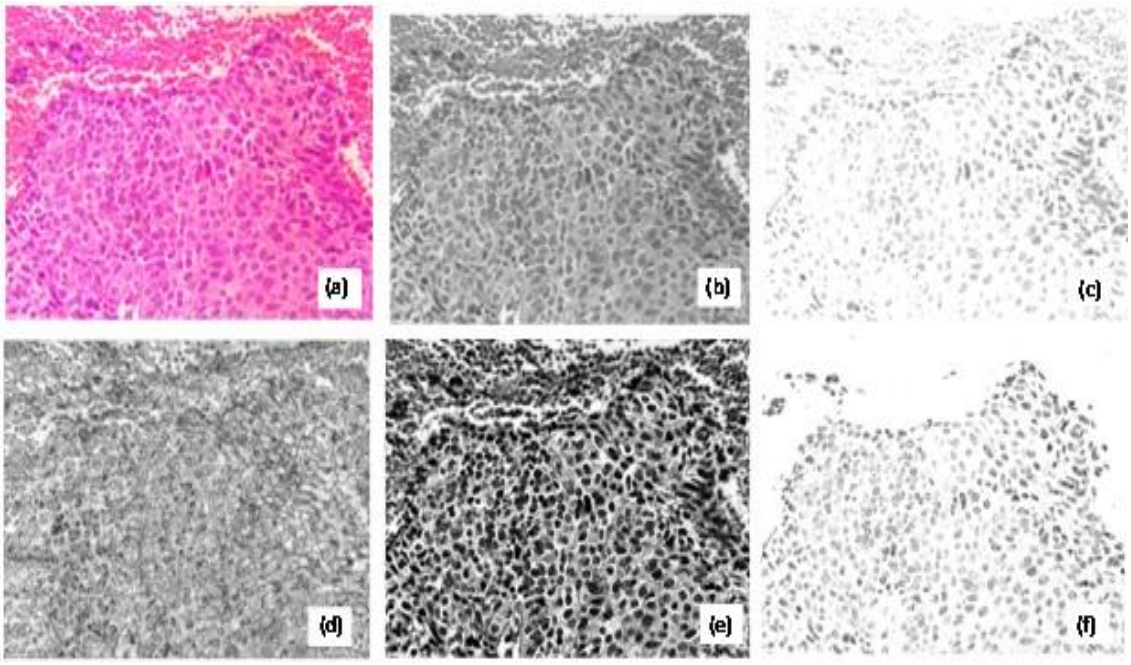


**Figure 3.11: Enhancement results using classical and proposed DSR method.**
(a) Photomicrograph of cervix cancer at 40× magnification. (b) Enhancement of intensity component of HSI image using (c) $\Upsilon$ correction with $\Upsilon$=1.1. (d) Single Scale Retinex (SSR) method. (e) CLAHE method. (f) DSR method.

The proposed image segmentation technique was tested on many histopathological images of cervix, ovarian, prostate and breast cancer respectively. The figure 3.12 (a) depicts the RBC and cancerous cells that belong to the original images. Hematoxylin and Eosin (HE) staining produced a very slight color difference between blood cells and cancerous cells. The figure 3.12 (b) shows proposed DSR method based suppression of the RBC and background staining while preserving the cancerous cells. Further, in figure 3.12 (c) depicts the automatic thresholding segmented cancerous cells from the blood cells.

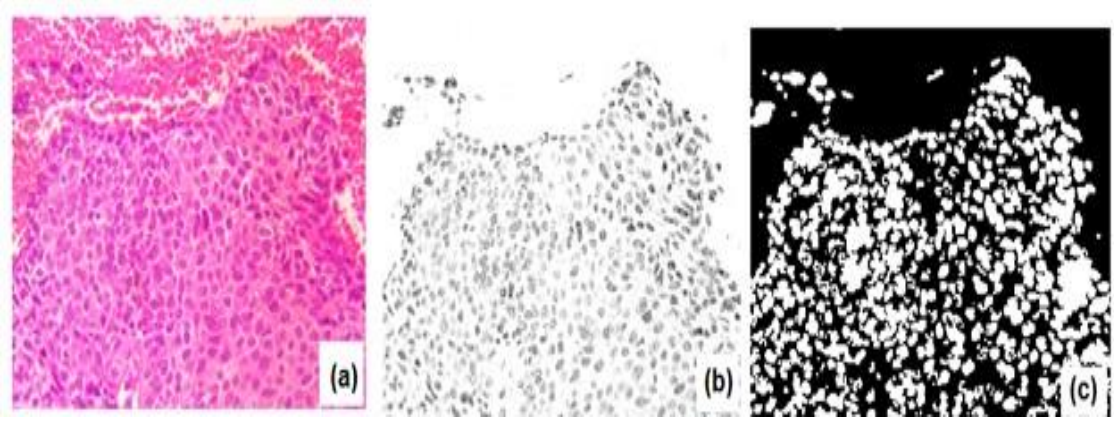


**Figure 3.12: Segmentation results of DSR processed image using Otsu's thresholding of cervix cancer obtained at 40× magnification.**
(a) Photomicrograph of cervix cancer. (b) Image obtained using DSR on intensity component, (c) Segmented cells from the image.

After the aforementioned steps, the proposed methodology was tested for the detection of different types of cancerous cells. The figure 3.13 (a) depicts the 100× magnification of the cervix cancer. The figure 3.13 (b) shows the image enhancement using proposed DSR technique. The figure 3.13 (c) shows image enhancement technique induced better segmentation of cervix cancerous cells. Eventually, the irregular shape and presence of more than one nucleus in the segmented image (as shown with the ellipse) confirms the malignant stage of cancer.

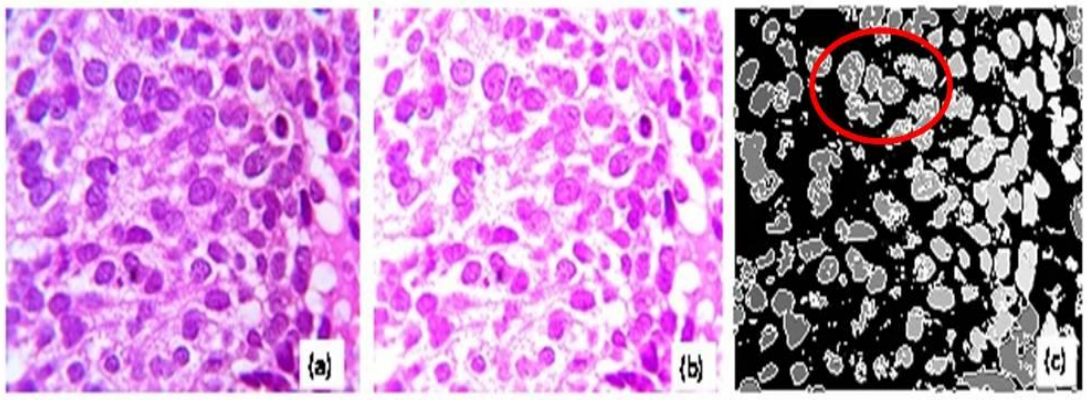


**Figure 3.13: Segmentation results of DSR processed image using Otsu's thresholding of cervix cancer obtained at 100× magnification.**
(a) Photomicrograph of cervix cancer. (b) Image enhancement using DSR. (c) Segmented cells from the image.

The image as shown in figure 3.14 (a) has been obtained using the 100× magnifications of prostate cancer. In this case, the cells were lightly stained and had poor boundaries, which makes it tough to segment cells from the background. The image present in figure 3.14 (c) reveals that all the cells are segmented accurately with least presence of background effect.

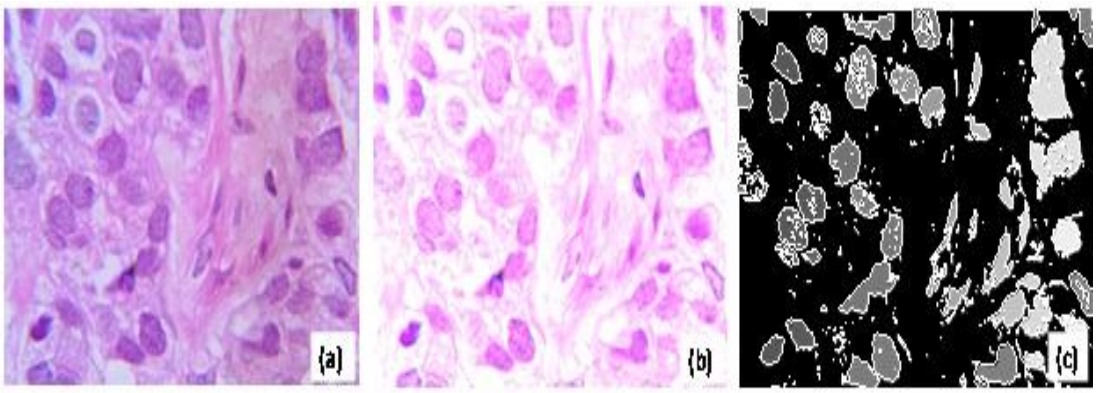


**Figure 3.14: Segmentation results of DSR processed image using Otsu's thresholding of prostate cancer obtained at 100× magnification.**
(a) Photomicrograph of the prostate cancer. (b) Image enhancement using DSR. (c) Segmented cells from the image.

The image as shown in figure 3.15 (a) has been obtained using the 100× magnifications of ovarian cancer where some of the cells are very lightly stained and some are highly stained. As shown in figure 3.15 (b), enhanced images where the contrast is increased, and the cells appeared clearer.

The intensity component of this enhanced image helps to make better segmentation. As shown in figure 3.15 (c) more than one nucleus present in the cells confirms the malignant stage of ovary cancer.

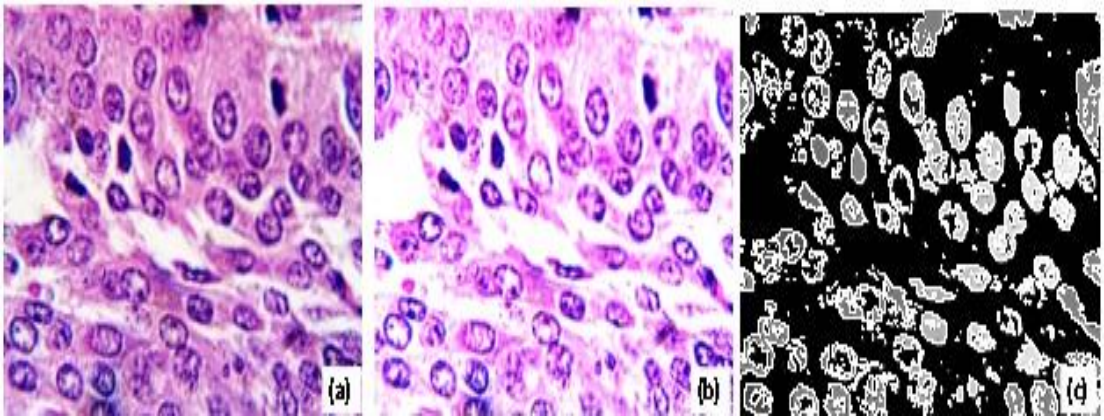


**Figure 3.15: Segmentation results of DSR processed image using Otsu's thresholding of ovarian cancer obtained at 100× magnification.**
(a) Photomicrograph of ovarian cancer. (b) Image enhancement using DSR, (c) Segmented cells from the image.

The comparison of segmentation results was performed on publically available datasets of breast cancer images obtained from www.bioimage.ucsb.edu (Centre for Bio-image Informatics, University of California, Santabarbara (UCSB) for analysis. The algorithm has been applied to total twenty-two (22) breast cancer images including benign and malignant with ROI segmented ground truth images to validate the performance of our proposed DSR based Ostu's thresholding method.

The figure 3.16 (benign-1), 3.17 (benign-2)and figure 3.18 (malignant-1), 3.19 (malignant-2) shows qualitative comparison among (c) automatic thresholding based Otsu's method (Kittler *et al.,* 1985), (d) k-means (Chen *et al.,* 1998; Kailasanathan *et al.,* 2001), (e) fuzzy c-means (Lim *et al.,* 1990; Ahmed *et al*., 1999; Pham *et al.,* 1999) and (f) proposed DSR based segmentation method for benign breast and malignant breast cells respectively. Cells present in the images shown in figure 3.16, 3.17 (f) for benign and figure 3.18, 3.19 (f) for malignant have clearer boundaries and closely related to the ground truth images using DSR based segmentation method.

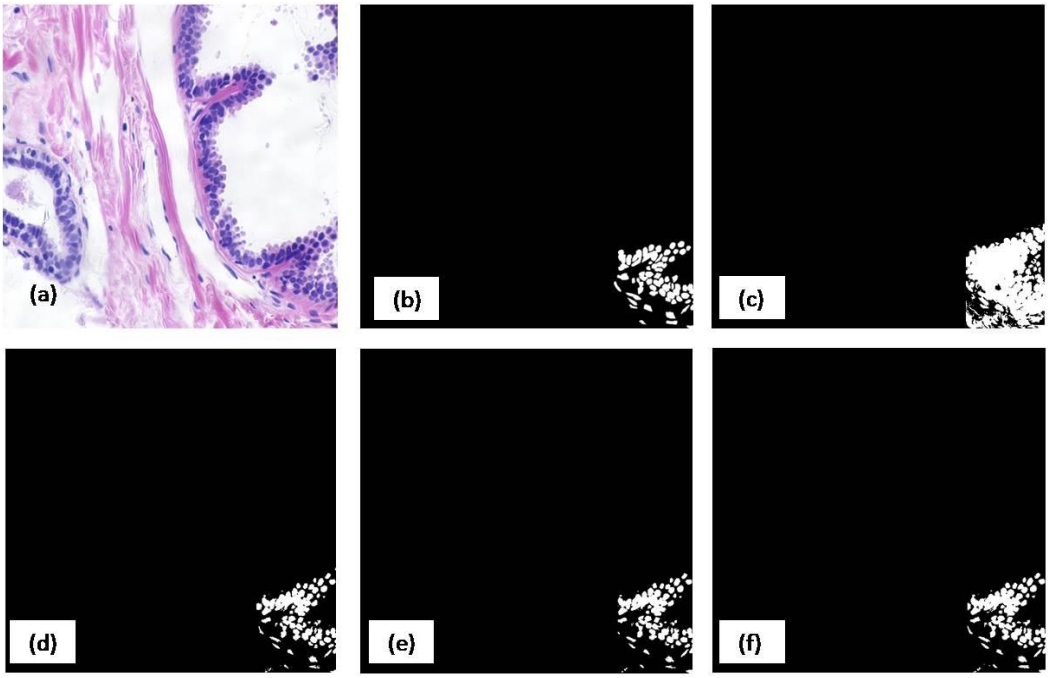


**Figure 3.16: Comparative segmentation results of (Benign 1).**
**(**a) Photomicrograph of the benign stage of breast cancer (b) Ground truth image. (c) Otsu's thresholding method. (d) k-means clustering method. (e) Fuzzy c-means method (f) Proposed DSR based Otsu's thresholding method.

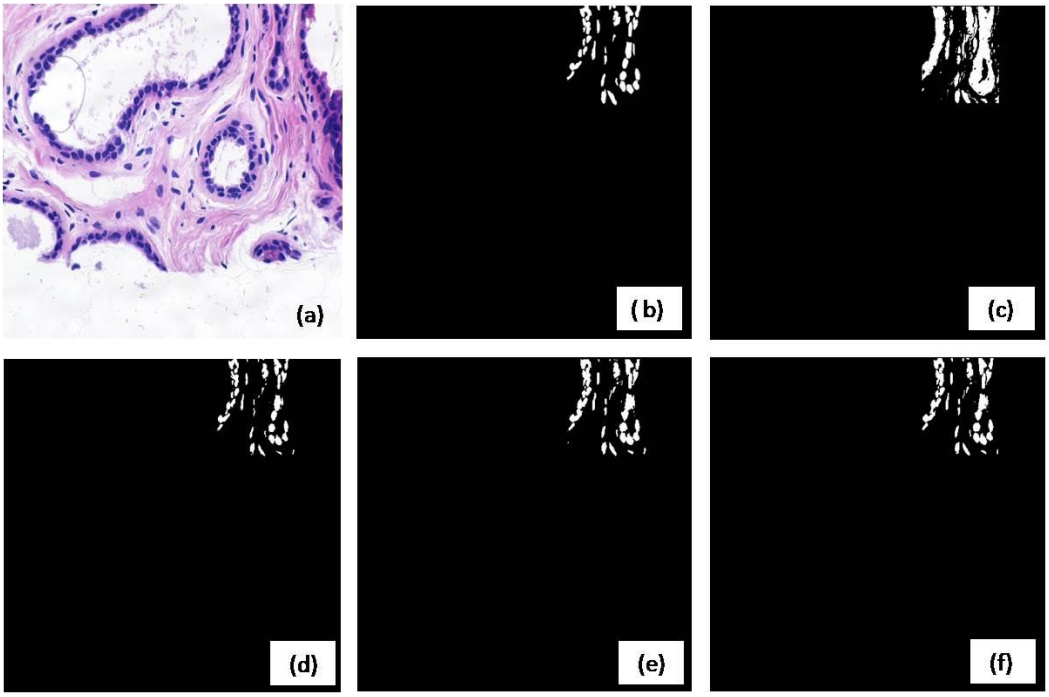


**Figure 3.17: Comparative segmentation results of (Benign 2).**
(a) Photomicrograph of the benign stage of breast cancer (b) Ground truth image. (c) Otsu's thresholding method. (d) k-means clustering method. (e) Fuzzy c-means method. (f) Proposed DSR based Otsu's thresholding method.

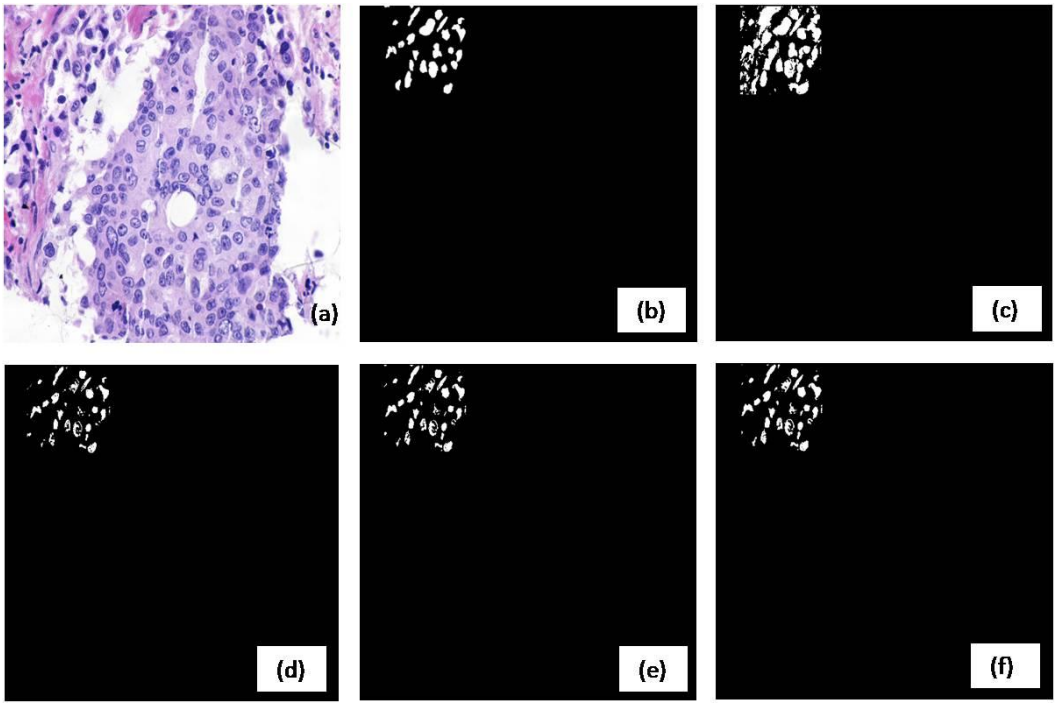


**Figure 3.18: Comparative segmentation results of (Malignant 1).**
(a) Photomicrograph of the malignant stage of breast cancer (b) ground truth image. (c) Otsu's thresholding method. (d) k-means clustering method. (e) Fuzzy c-means method. (f) Proposed DSR based Otsu's thresholding method.

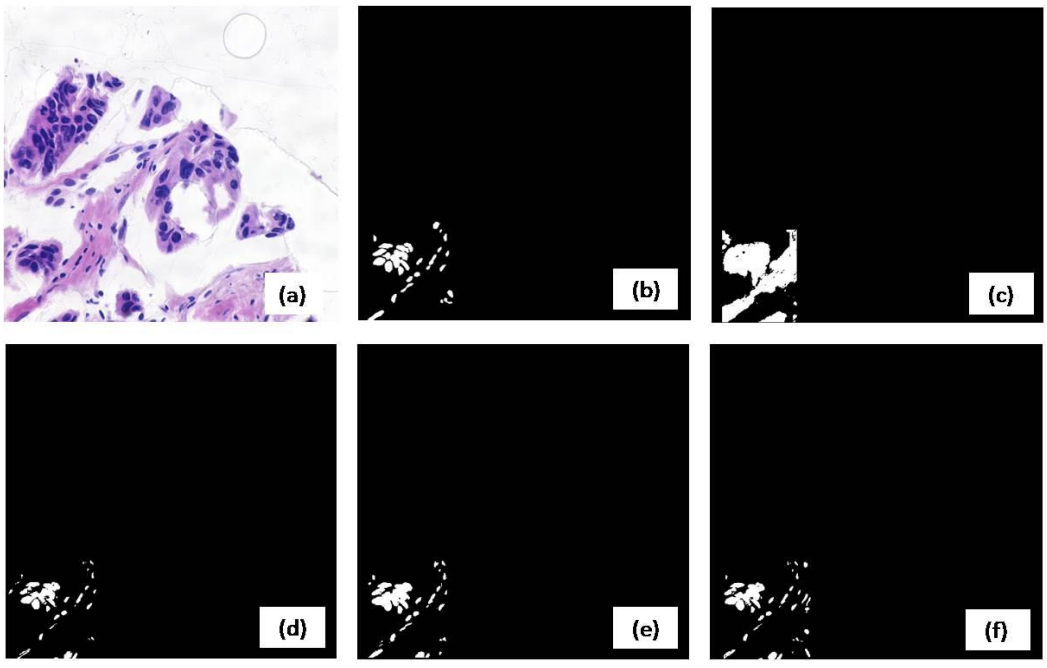


**Figure 3.19: Comparative segmentation results of (Malignant 2).**
(a) Photomicrograph of the malignant stage of breast cancer. (b) Ground truth image. (c) Otsu's thresholding method. (d) k-means clustering method, (e) Fuzzy c-means method (f) Proposed DSR based Otsu's thresholding method.

Segmentation is quantified in terms of **(a)** correlation, **(b)** NPR index (Unnikrishnan *et al.,* 2005), **(c)** VI (Unnikrishnan *et al.,* 2007) and **(d)** GCE (Martin *et al.,* 2001) of the segmented image with the ground truth image. GCE and VI should be low, whereas correlation and NPR should be high for a better-segmented image. The results have shown in table 3.1 (Ostu's thresholding), 3.2 (k-means clustering), 3.3 (fuzzy c-mean), reveals that Otsu's method, k-means method, and fuzzy c-means method have high GCE and VI whereas low NPR index and correlation in comparison to proposed method presented in table 3.4. This phenomenon shows the edge of proposed method (DSR technique) over conventional methods in terms of segmentation performance.

Table 3.1, 3.2, 3.3, and 3.4 represent information of Otsu's method, k-means method, and fuzzy c-means method and proposed DSR based Otsu's thresholding method respectively. The Table 3.1 to 3.4 contains the finding reports that include the proposed method based tests conducted over 22 histopathological images of breast cancer for performance validation.

**Table 3.1: Quantitative evaluation of Ostu's thresholding segmentation methods for 22 images.**

| Segmentation Method | Sample image | Performance measure | | | |
|---|---|---|---|---|---|
| | | Correlation (Higher better) | NPR (Higher better) | GCE (Lower better) | VI (Lower better) |
| Ostu's thresholding | 1test image (Benign 1) | 0.6365 | 0.9491 | 0.0337 | 0.3286 |
| | 2 test image (Benign 2) | 0.6842 | 0.9771 | 0.0206 | 0.195 |
| | 3 test image (Malignant 1) | 0.71 | 0.976 | 0.0202 | 0.1889 |
| | 4 test image (Malignant 2) | 0.5164 | 0.9624 | 0.0212 | 0.2349 |
| | 5 image | 0.726 | 0.9789 | 0.0194 | 0.1912 |
| | 6 image | 0.3547 | 0.9392 | 0.0328 | 0.3413 |
| | 7 image | 0.6191 | 0.9526 | 0.0377 | 0.3422 |
| | 8 image | 0.6661 | 0.9752 | 0.0215 | 0.2272 |
| | 9 image | 0.5474 | 0.9582 | 0.0206 | 0.2488 |
| | 10 image | 0.7081 | 0.9612 | 0.0361 | 0.3159 |
| | 11 image | 0.6087 | 0.9449 | 0.0393 | 0.377 |
| | 12 image | 0.644 | 0.966 | 0.0244 | 0.2404 |
| | 13 image | 0.4936 | 0.9332 | 0.0362 | 0.394 |
| | 14 image | 0.5788 | 0.9616 | 0.0208 | 0.2356 |
| | 15 image | 0.586 | 0.9436 | 0.0299 | 0.3224 |
| | 16 image | 0.5786 | 0.966 | 0.0192 | 0.2142 |
| | 17 image | 0.5798 | 0.948 | 0.0275 | 0.3022 |
| | 18 image | 0.6022 | 0.9548 | 0.0308 | 0.306 |
| | 19 image | 0.4445 | 0.9323 | 0.0353 | 0.3909 |
| | 20 image | 0.4684 | 0.9351 | 0.0419 | 0.4163 |
| | 21 image | 0.5964 | 0.958 | 0.0326 | 0.3053 |
| | 22 image | 0.4693 | 0.9426 | 0.021 | 0.2942 |
| | Average value | 0.58267 | 0.955273 | 0.028305 | 0.291477 |

**Table 3.2: Quantitative evaluation of k-means clustering segmentation methods for 22 images.**

| Segmentation Method | Sample image | Performance measure | | | |
|---|---|---|---|---|---|
| | | **Correlation (Higher better)** | **NPR (Higher better)** | **GCE (Lower better)** | **VI (Lower better)** |
| **K -mean clustering** | 1 test image (Benign 1) | 0.8187 | 0.9783 | 0.0111 | 0.2097 |
| | 2 test image (Benign 2) | 0.8744 | 0.9872 | 0.0037 | 0.1281 |
| | 3 test image (Malignant 1) | 0.7457 | 0.9821 | 0.007 | 0.1495 |
| | 4 test image (Malignant 2) | 0.7751 | 0.9861 | 0.0061 | 0.1259 |
| | 5 image | 0.7627 | 0.985 | 0.0042 | 0.1301 |
| | 6 image | 0.686 | 0.9627 | 0.0127 | 0.2716 |
| | 7 image | 0.8277 | 0.9741 | 0.0096 | 0.2341 |
| | 8 image | 0.6321 | 0.9761 | 0.0081 | 0.1819 |
| | 9 image | 0.6749 | 0.9708 | 0.0122 | 0.2381 |
| | 10 image | 0.7343 | 0.9839 | 0.0055 | 0.1362 |
| | 11 image | 0.7837 | 0.9799 | 0.0123 | 0.1925 |
| | 12 image | 0.8243 | 0.988 | 0.0051 | 0.1138 |
| | 13 image | 0.7008 | 0.9765 | 0.0107 | 0.1909 |
| | 14 image | 0.7373 | 0.9752 | 0.0111 | 0.2088 |
| | 15 image | 0.5601 | 0.9673 | 0.0137 | 0.2472 |
| | 16 image | 0.7916 | 0.9728 | 0.0156 | 0.2522 |
| | 17 image | 0.7951 | 0.9781 | 0.0146 | 0.2109 |
| | 18 image | 0.8737 | 0.9913 | 0.0045 | 0.1078 |
| | 19 image | 0.5464 | 0.972 | 0.0063 | 0.1873 |
| | 20 image | -0.0051 | 0.9587 | 0.0054 | 0.2284 |
| | 21 image | 0.7049 | 0.9655 | 0.0219 | 0.28 |
| | 22 image | 0.7507 | 0.9777 | 0.0078 | 0.1882 |
| | Average value | 0.70887 | 0.976786 | 0.009509 | 0.191509 |

**Table 3.3: Quantitative evaluation of Fuzzy c-means clustering segmentation methods for 22 images.**

| Segmentation Method | Sample image | Performance measure | | | |
|---|---|---|---|---|---|
| | | Correlation (Higher better) | NPR (Higher better) | GCE (Lower better) | VI (Lower better) |
| **Fuzzy c-mean clustering** | 1 test image (Benign 1) | 0.8207 | 0.9785 | 0.0104 | 0.2096 |
| | 2 test image (Benign 2) | 0.8731 | 0.9896 | 0.0055 | 0.1234 |
| | 3 test image (Malignant 1) | 0.7772 | 0.9838 | 0.0072 | 0.1451 |
| | 4 test image (Malignant 2) | 0.843 | 0.9897 | 0.0061 | 0.1132 |
| | 5 image | 0.7953 | 0.987 | 0.0071 | 0.1333 |
| | 6 image | 0.7775 | 0.9697 | 0.0137 | 0.2554 |
| | 7 image | 0.8489 | 0.9787 | 0.0133 | 0.2296 |
| | 8 image | 0.6046 | 0.975 | 0.0084 | 0.1864 |
| | 9 image | 0.7075 | 0.9687 | 0.0234 | 0.2609 |
| | 10 image | 0.7345 | 0.9838 | 0.0066 | 0.1403 |
| | 11 image | 0.7376 | 0.9745 | 0.0225 | 0.2205 |
| | 12 image | 0.8423 | 0.99 | 0.0063 | 0.1101 |
| | 13 image | 0.7639 | 0.9786 | 0.0154 | 0.1904 |
| | 14 image | 0.7497 | 0.9747 | 0.018 | 0.2223 |
| | 15 image | 0.6438 | 0.9705 | 0.0174 | 0.245 |
| | 16 image | 0.7018 | 0.9621 | 0.0337 | 0.3042 |
| | 17 image | 0.7622 | 0.9748 | 0.0217 | 0.2285 |
| | 18 image | 0.6858 | 0.9815 | 0.017 | 0.1633 |
| | 19 image | 0.592 | 0.9736 | 0.007 | 0.1837 |
| | 20 image | 0.7705 | 0.9811 | 0.0117 | 0.1741 |
| | 21 image | 0.7215 | 0.969 | 0.0194 | 0.2664 |
| | 22 image | 0.7663 | 0.9787 | 0.0101 | 0.1928 |
| | Average value | 0.75089 | 0.977891 | 0.013723 | 0.195386 |

**Table 3.4: Quantitative evaluation of proposed DSR based Otsu's thresholding segmentation methods for 22 images.**

| Segmentation Method | Sample image | Performance measure | | | |
|---|---|---|---|---|---|
| | | **Correlation (Higher better)** | **NPR (Higher better)** | **GCE (Lower better)** | **VI (Lower better)** |
| **Proposed DSR based Otsu's thresholding method** | 1 test image (Benign 1) | 0.8373 | 0.9802 | 0.0108 | 0.2054 |
| | 2 test image (Benign 2) | 0.8935 | 0.9903 | 0.0046 | 0.1219 |
| | 3 test image (Malignant 1) | 0.8034 | 0.9846 | 0.0081 | 0.1457 |
| | 4 test image (Malignant 2) | 0.8568 | 0.9905 | 0.0051 | 0.1078 |
| | 5 image | 0.8137 | 0.9872 | 0.0052 | 0.1271 |
| | 6 image | 0.7673 | 0.9687 | 0.0128 | 0.2551 |
| | 7 image | 0.8526 | 0.9778 | 0.0113 | 0.2283 |
| | 8 image | 0.637 | 0.9762 | 0.0081 | 0.1815 |
| | 9 image | 0.7251 | 0.9724 | 0.0167 | 0.2418 |
| | 10 image | 0.7381 | 0.9839 | 0.0061 | 0.1383 |
| | 11 image | 0.7676 | 0.9783 | 0.0173 | 0.2042 |
| | 12 image | 0.8332 | 0.9885 | 0.0064 | 0.1143 |
| | 13 image | 0.7867 | 0.9806 | 0.0113 | 0.1778 |
| | 14 image | 0.7466 | 0.9751 | 0.0157 | 0.2186 |
| | 15 image | 0.6109 | 0.9692 | 0.0152 | 0.2447 |
| | 16 image | 0.788 | 0.9739 | 0.0193 | 0.2541 |
| | 17 image | 0.7744 | 0.977 | 0.0189 | 0.2205 |
| | 18 image | 0.7921 | 0.9876 | 0.0097 | 0.131 |
| | 19 image | 0.7062 | 0.9786 | 0.0089 | 0.1733 |
| | 20 image | 0.7426 | 0.9763 | 0.0209 | 0.1968 |
| | 21 image | 0.8216 | 0.9781 | 0.0115 | 0.218 |
| | 22 image | 0.7916 | 0.9802 | 0.0079 | 0.1813 |
| | Average value | 0.77665 | 0.979782 | 0.011445 | 0.185795 |

(NPR -Normalized Probabilistic Rand, GCE - Global Consistency Error, VI - Variation of Information)

The figure 3.20 depicts the mean and standard deviations of correlation, GCE, NPR and VI for total 22 images (including benign and malignant cancer) respectively. It is evident that correlation and NPR are highest for proposed method whereas VI is lowest than the other competing methods. However, k-means based segmentation has slightly more GCE than the proposed algorithm. The least standard deviation of correlation, GCE, NPR, and VI obtained using proposed algorithm showing its highest consistency of segmentation irrespective of input image quality.

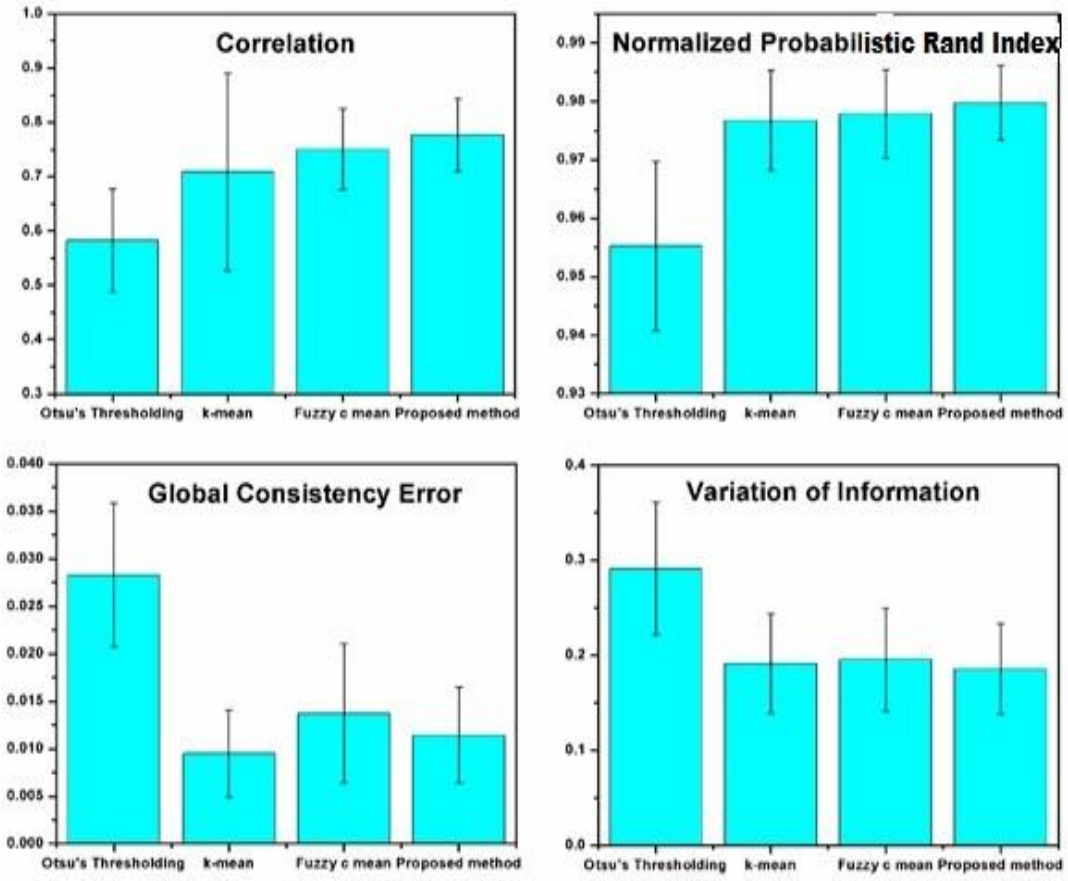


**Figure 3.20: Comparison of Otsu's thresholding, k-mean, fuzzy c-mean and proposed DSR segmentation methods for 22 images.**

(a) Correlation (b) Normalized probabilistic rand index (c) Global consistency error (d) Variation of information. Statistical analysis has been performed using Origin (Ver.8, Origin Lab Corporation, UK) were used in this study. The results presented here are expressed as Mean ± S.D.

DSR technique in discrete cosine transform based segmentation is proposed for the enhancement and segmentation of cells of histopathological images. Some existing image segmentation algorithms were compared with proposed methodology (DSR). The experimental results reveal that these Otsu's method, k-means method, and fuzzy c-means method are not suitable to get adequate cell segmentation for noisy images. Besides, the performance of these algorithms degrades for objects having the similar background. At this point, our proposed DSR based technique produces better image enhancement and restoration of essential information.

## 3.6 Conclusion:

The motivation of this chapter was to investigate the neutralization of noise because of the lack of illumination using the internal noise itself. DSR in the spatial domain enhances for the segmentation of low contrast histopathological images. This technique tunes the intensity values of the image according to the Quartic Bi-stable double-well system parameters $a$ and $b$ and utilizes internal noise for the enhancement. The iterative process facilitates the transition of the image from low contrast to good contrast state, which finally yielded better segmentation. The segmented output images of proposed algorithm have been compared with the processed images of existing Otsu's threshold, k-means, and fuzzy c-means techniques. It has been quantitatively found that the segmented image has high correlation and less mismatched pixels with ground truth image for the proposed method. The main advantage of proposed algorithm is that it deals with only intensity component of a colour model, which was processed with DSR, based technique. The DSR based proposed approach associated with the high value of correlation and NPR with the low value of GCE and VI in comparison to other methods. The proposed DSR based Otsu’s thresholding segmentation method perform better than other methods and shows recommendable potential for feature extraction of images in cancer cell detections. DSR demonstrated very impressive performance to enhance low contrast histopathology images